nature chemical biology

ARTICLE

PUBLISHED ONLINE: 15 MAY 2017 | DOI: 10.1038/NCHEMBIO.2374

β-Lactone formation during product release from a nonribosomal peptide synthetase

Jason E Schaffer[1,2], Margaret R Reck[1,2], Neha K Prasad[1] & Timothy A Wencewicz[1]*

Nonribosomal peptide synthetases (NRPSs) are multidomain modular biosynthetic assembly lines that polymerize amino acids into a myriad of biologically active nonribosomal peptides (NRPs). NRPS thioesterase (TE) domains employ diverse release strategies for off-loading thioester-tethered polymeric peptides from termination modules typically via hydrolysis, aminolysis, or cyclization to provide mature antibiotics as carboxylic acids/esters, amides, and lactams/lactones, respectively. Here we report the enzyme-catalyzed formation of a highly strained β-lactone ring during TE-mediated cyclization of a β-hydroxythioester to release the antibiotic obafluorin (Obi) from an NRPS assembly line. The Obi NRPS (ObiF) contains a type I TE domain with a rare catalytic cysteine residue that plays a direct role in β-lactone ring formation. We present a detailed genetic and biochemical characterization of the entire Obi biosynthetic gene cluster in plant-associated *Pseudomonas fluorescens* ATCC 39502 that establishes a general strategy for β-lactone biogenesis.

© 2017 Nature America, Inc., part of Springer Nature. All rights reserved.

Strained β-lactone rings are found in diverse classes of natural products, including polyketides (PKs), nonribosomal peptides (NRPs), amino acids, terpenoids, and hybrid molecules[1]. Little is known about the biosynthetic origins of β-lactones despite the wide therapeutic value of naturally occurring β-lactones as inhibitors of enzymes in the serine hydrolase superfamily[2]. Tetrahydrolipstatin is a hybrid PK–NRP lipase inhibitor, known commercially as Orlistat, that is approved by the US Food and Drug Administration for the treatment of obesity[3]. Salinosporamide A, also known as marizomib and NPI-0052, is a hybrid PK–NRP proteasome inhibitor that is under clinical investigation for use as a treatment of multiple myeloma and other advanced malignancies[4]. Other natural β-lactones show promise as antimicrobial[5], anticancer[4], antiviral[6], and anti-obesity[3] agents (**Supplementary Results**, **Supplementary Fig. 1**). The genetic and biochemical basis for β-lactone ring formation is an unsolved problem in natural product biosynthesis[7].

There is a precedent for enzymatic formation of strained four-membered rings in the closely related β-lactam family of antibiotics[8]. Three chemically distinct biosynthetic pathways leading to β-lactams have been reported. Penicillin and cephalosporin bicyclic β-lactam scaffolds form via oxidative cyclization of an NRP tripeptide precursor by isopenicillin N synthase[9]. The β-lactam rings in clavulanic acid and carbapenems arise via ATP-dependent cyclization of β-amino acid precursors catalyzed by the β-lactam synthetase enzyme family[10]. The nocardicin family of monocyclic β-lactam antibiotics are derived from an NRPS assembly line comprised of five catalytic modules that each covalently tether the evolving substrate in the form of a thioester on a peptidyl carrier protein, also known as the thiolation (T) domain. The condensation (C) domain of module 5 has a rare HHHxxDG motif that is important for dehydration of a T_4-serine thioester to a T_4-dehydroalanine thioester electrophile that undergoes a Michael addition–nucleophilic acyl substitution reaction cascade with the nucleophilic α-amino group of a downstream T_5-L-(*p*-hydroxyphenyl)glycine thioester to produce the nocardicin β-lactam warhead[11]. We hypothesized that similar biosynthetic strategies could conceivably be employed to assemble β-lactone rings.

The β-lactone synthetase enzyme OleC produces β-lactone intermediates during olefinic hydrocarbon biosynthesis[12]. OleC is proposed to catalyze the ATP-dependent cyclization of *syn* and *anti* β-hydroxy acids to the corresponding *cis* and *trans* β-lactones, which undergo decarboxylation to give the *cis* and *trans* double bonds found in olefinic hydrocarbons. The biosynthetic gene clusters for the natural product β-lactones lipstatin[13], ebelactone[7], salinosporamide[14], and oxazolomycin[15] are known, and their biosynthetic pathways have been proposed. However, the mechanisms for β-lactone ring formation in these systems remain unclear, and no enzyme domains have been experimentally linked to β-lactone cyclization. Interestingly, the terminating PKS or NRPS module for each β-lactone antibiotic lacks an embedded TE domain[16]. TE domains can participate in acyl transfers[17], epimerization of stereogenic centers[18], proofreading[19], and product release via hydrolysis or macrocyclization[20]. The β-lactone rings of lactacystin and ebelactone can form nonenzymatically at pH 7 from precursor β-hydroxythioesters, which challenges the evolutionary need for enzyme catalysis of β-lactone ring formation[7,21]. We hypothesized that enzyme catalysis could still be at play for these β-lactones, a factor that might have been overlooked as a result of the relative stability of the β-lactones. Thus, we turned our search for a 'β-lactone synthase' to scenarios in which the β-lactone is rapidly hydrolyzed in aqueous environments, where enzyme catalysis would be needed to increase the rate of β-lactone ring formation to maintain titer levels that are beneficial to the producing microbe.

We discovered that enzyme catalysis is required for strained ring formation during biosynthesis of the NRPS β-lactone antibiotic obafluorin (Obi, **1**), which rapidly hydrolyzes to the corresponding β-hydroxycarboxylic acid (Obi-COOH, **2**) at neutral pH[22,23]. We used full genome sequencing and comparative sequence analysis to identify a putative Obi biosynthetic gene cluster in the known Obi producer *P. fluorescens* ATCC 39502. We biochemically characterized five recombinant enzymes, ObiD, ObiF, ObiG, ObiH, and ObiL, that convert chorismate-derived 2,3-dihydroxybenzoic acid (2,3-DHB, **3**) and *p*-NH_2-phenylpyruvic acid (PAPPA, **4**) to Obi by way of the biosynthetic intermediates *p*-NO_2-phenylpyruvic acid (PNPPA, **5**), *p*-NO_2-phenylacetaldehyde (PNPAA, **6**), and (*R*)-β-hydroxy-*p*-nitro-L-homophenylalanine (β-OH-*p*-NO_2-homoPhe, **7**). We found that the type I TE domain of ObiF catalyzed the cyclization of an active site–tethered Cys-β-hydroxythioester during product

[1]Department of Chemistry, Washington University in St. Louis, St. Louis, Missouri, USA. [2]These authors contributed equally to this work.
*e-mail: wencewicz@wustl.edu

release from the NRPS assembly line. Our findings establish a genetic signature and biochemical mechanism for β-lactone biosynthesis from NRPS assembly lines that will guide future β-lactone natural product discovery efforts through genome mining, computational structure prediction, chemoenzymatic synthesis, and directed biosynthesis[24,25].

RESULTS

Identification of the obafluorin biosynthetic gene cluster

Obi is a *cis*-monocyclic β-lactone antibiotic produced by plant-associated strains of *P. fluorescens*[22,23]. Under physiological conditions, Obi spontaneously hydrolyzes to the corresponding β-hydroxycarboxylic acid Obi-COOH (**Fig. 1a**)[26]. The unique structure of Obi contains a 2,3-DHB unit coupled through an amide linkage to an α-amino-β-lactone ring of the unusual nonproteinogenic amino acid β-OH-*p*-NO_2-homoPhe. Stable-isotope feeding studies suggest that 2,3-DHB and β-OH-*p*-NO_2-homoPhe are advanced intermediates in the biosynthesis of Obi[27,28]. We sequenced the genome of the known Obi producer *P. fluorescens* ATCC 39502 to search for a putative Obi biosynthetic gene cluster. We identified a ~20-kilobase-pair gene cluster with 14 candidate coding sequences (CDSs), including one encoding an AurF di-iron nonheme arylamine oxygenase homolog (*obiL*) predicted to install the aryl nitro functional group via oxidation of the precursor aniline (**Fig. 1b** and **Supplementary Table 1**). The Obi gene cluster encodes putative enzymes required for the biosynthesis of 2,3-DHB (*obiA*, *obiB*, *obiC*, and *obiE*) and the nonproteinogenic amino acid β-OH-*p*-NO_2-homoPhe (*obiG*, *obiH*, *obiI*, *obiJ*, *obiK*, and *obiL*). CDSs encoding an aryl acyl carrier protein (*obiD*) and an NRPS module (*obiF*) with condensation (C), acid adenylation (A), aryl acid adenylation (A_{Ar}), thiolation (T), and thioesterase (TE) domains make up the remaining biosynthetic genes. There are no obvious antibiotic resistance genes in the cluster. The genes *obiM* and *obiN* encode proteins that have strong homology to the acylhomoserine lactone (AHL) synthase LuxI and the AHL-binding transcriptional regulator LuxR, respectively. The LuxI and LuxR pair is a common quorum-sensing system found in many pseudomonads. A basic local alignment search tool (BLAST) search of the NCBI database revealed homologous Obi clusters in other pseudomonads including *Pseudomonas* sp. 37_R_15 and 34_E_7, the environmental chitin-degrading bacterium *Chitiniphilus shinanonensis* SAY3, and the plant-growth-promoting rhizobacterium *Burkholderia diffusa* RF8-non_BP2, which is also an opportunistic human pathogen (**Supplementary Table 2**; **Supplementary Figs. 2** and **3**).

2,3-DHB and PAPPA are precursors to Obi

Chorismate is the primary carbon source of the Obi biosynthetic pathway (**Supplementary Fig. 4a**)[27,28]. The gene *obiB* encodes an extra copy of the first biosynthetic enzyme from the shikimate pathway, 3-deoxy-D-arabinoheptulosonate-7-phosphate (DAHP) synthase, which converts phosphoenolpyruvate (PEP) and erythrose-4-phosphate to chorismate[29]. Chorismate is converted to 2,3-DHB by isochorismate synthase (ObiA), isochorismatase (ObiE), and a dehydrogenase (ObiC), which are analogous to EntC, EntB, and EntA, respectively, involved in biosynthesis of the siderophore enterobactin[30]. Chorismate is also converted to PAPPA by the 4-amino-4-deoxychorismate (4-ADC) synthase (ObiJ and ObiK) and 4-ADC mutase/dehydratase (ObiI), a process analogous to that of the CmlB, CmlC, and CmlD and PapA, PapB, and PapC enzymes that lead to PAPPA in the chloramphenicol[31] and pristinamycin[32] biosynthetic pathways, respectively (**Supplementary Fig. 4b**). We undertook *in vitro* reconstitution of the remaining biosynthetic enzymes (ObiD, ObiF, ObiG, ObiH, and ObiL) to establish the timing and action of each step in the conversion of 2,3-DHB and PAPPA to Obi (**Supplementary Fig. 5**).

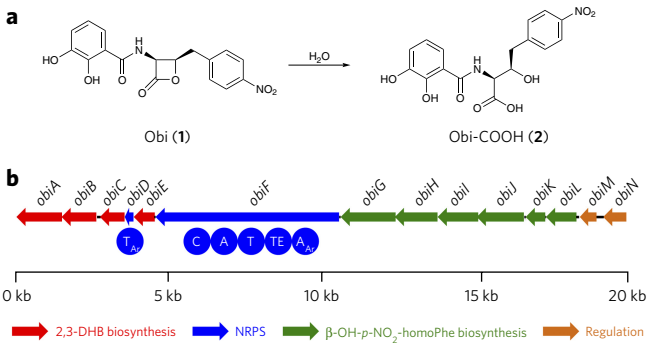

Figure 1 | Biosynthetic gene cluster for obafluorin β-lactone from *P. fluorescens* ATCC 39502. (**a**) Obafluorin β-lactone (Obi) undergoes nonenzymatic hydrolysis to form a β-hydroxycarboxylic acid (Obi-COOH). (**b**) Annotated biosynthetic gene cluster of Obi identified from whole-genome sequencing of *P. fluorescens* ATCC 39502. Arrows represent coding sequences. A, acid adenylation; A_{Ar}, aryl acid adenylation; C, condensation; T, acid thiolation; T_{Ar}, aryl acid thiolation; TE, thioesterase; NRPS, nonribosomal peptide synthetase.

Conversion of PAPPA to β-OH-*p*-NO_2-homoPhe

Three enzymes (ObiL, ObiG, and ObiH) are required to convert PAPPA to β-OH-*p*-NO_2-homoPhe (**Fig. 2a**). We found that ObiL, a putative nonheme di-iron oxygenase, catalyzed the six-electron oxidation of the arylamine PAPPA to the aryl nitro PNPPA. Related examples of arylamine oxidases are found in the biosynthetic pathways of aureothin (AurF; GenBank EJZ60582.1) and chloramphenicol (CmlI; PDB 5HYH). ObiL showed 24% and 18% sequence homology to AurF and CmlI, respectively (**Supplementary Table 3**; **Supplementary Fig. 6a**)[33,34]. Similarly to ObiL, AurF acts early in the biosynthetic pathway of aureothin to oxidize *p*-aminobenzoic acid (PABA) to *p*-nitrobenzoic acid (PNBA). CmlI catalyzes the oxidation of the penultimate aniline intermediate to the aryl nitro as the final step of chloramphenicol biosynthesis[34]. Treatment of recombinant ObiL with PAPPA under reaction conditions similar to those used to functionally characterize AurF resulted in an immediate color change of the reaction mixture from clear and colorless to sky blue (**Supplementary Fig. 7**)[33]. Subsequent treatment of the ObiL–PAPPA reaction mixture with recombinant ObiG and ObiH in the presence of thiamine diphosphate (ThDP), pyridoxal phosphate (PLP), and L-Thr produced β-OH-*p*-NO_2-homoPhe, which was detected by LC–MS (**Fig. 2b**). The results of the triple-enzyme ObiL–ObiG–ObiH reaction confirmed that all three recombinant enzymes were capable of converting PAPPA directly to β-OH-*p*-NO_2-homoPhe, but the timing of each reaction required further clarification.

We discovered that ObiG, a ThDP-dependent phenylpyruvate decarboxylase, catalyzed the conversion of PNPPA to PNPAA (**Fig. 2a**; **Supplementary Figs. 6b** and **8**). A colorimetric Purpald assay suggested that PNPPA is decarboxylated to the aldehyde PNPAA in the presence of ThDP and ObiG (**Supplementary Fig. 9**). A double-enzyme reaction with ObiG and ObiH in the presence of ThDP, PLP, and L-Thr revealed that PNPPA is directly converted to β-OH-*p*-NO_2-homoPhe, which was detected by LC–MS (**Fig. 2c**) and ^{1}H-NMR (**Fig. 2d**). PAPPA was not accepted as a substrate by ObiG and ObiH, suggesting that ObiL oxidized PAPPA before catalysis by ObiG and ObiH (**Fig. 2c,d** and **Supplementary Fig. 10**).

BLAST searches suggested that ObiH was a PLP-dependent threonine aldolase[35]. Similar aldolases are involved in the biosynthesis of natural products containing β-hydroxy-α-amino acids, including the peptidyl nucleoside antibiotics A090289 A, caprazamycin A, and muramycin A1 (ref. 36), the 4-methyl-oxazoline antibiotics JBIR-34

© 2017 Nature America, Inc., part of Springer Nature. All rights reserved.

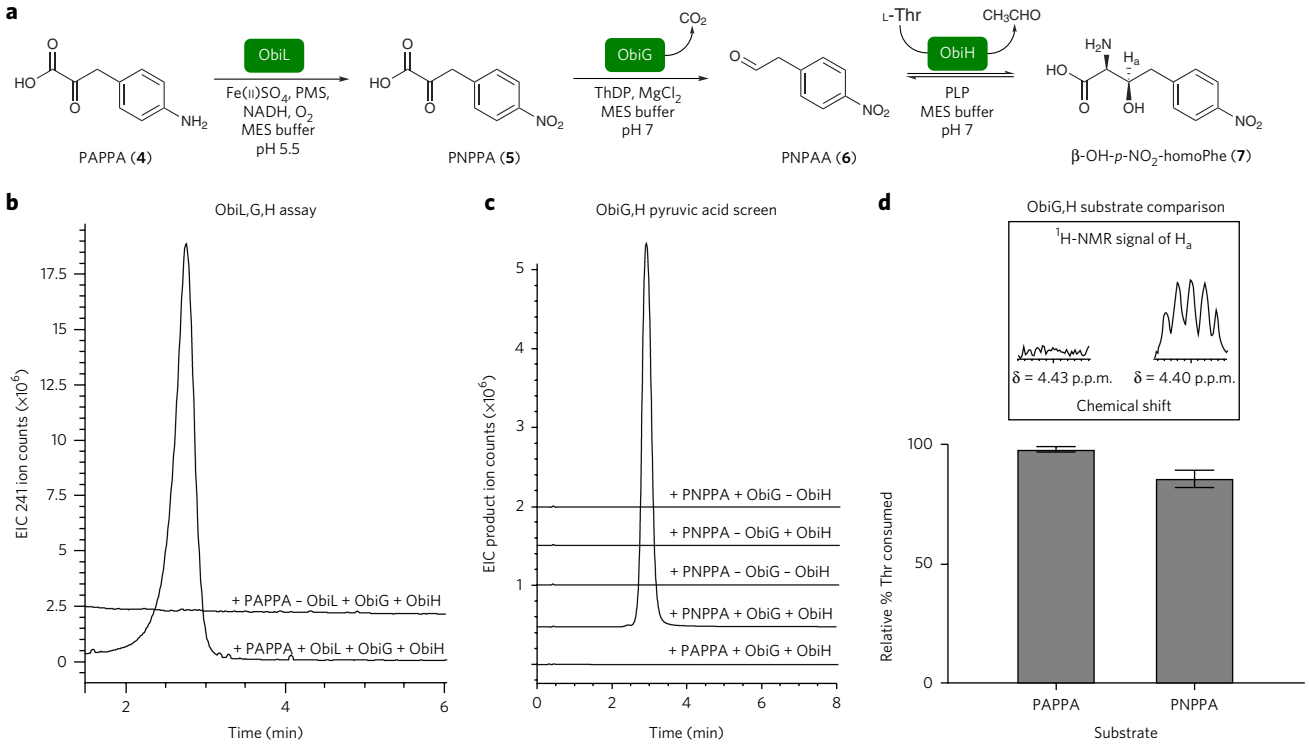

Figure 2 | Enzymatic conversion of PAPPA to β-OH-*p*-NO_2-homoPhe using recombinant oxidase ObiL, decarboxylase ObiG, and aldolase ObiH. (**a**) Scheme depicting the conversion of PAPPA to β-OH-*p*-NO_2-homoPhe by tandem actions of ObiL, ObiG, and ObiH. (**b**) Extracted ion chromatograms (EICs) (β-OH-*p*-NO_2-homoPhe $[M+H]^+$ ion *m/z* = 241) for the triple-enzyme reaction of PAPPA with ObiL, ObiG, and ObiH. PMS, phenazine methosulfate. (**c**) EICs for the double-enzyme reaction of PAPPA and PNPPA with ObiG and ObiH. EICs were generated by LC–MS in positive ion mode using single ion monitoring (SIM) for the predicted *m/z* values for the PAPPA (*m/z* = 211) and PNPPA (*m/z* = 241) product $[M+H]^+$ ions. Data represents a single measurement from two independent experiments. (**d**) The box shows a zoomed region of the ^{1}H-NMR spectra for the ObiG and ObiH double-enzyme reactions with L-Thr and PAPPA or PNPPA after 3 h of equilibration in which H_a on C3 of β-OH-*p*-NO_2-homoPhe appears as a doublet of doublet of doublets. The bar graph depicts the relative percent of L-Thr remaining for each reaction, based on integration of the L-Thr methyl signal in the ^{1}H-NMR spectra. Error bars represent s.d. for three independent trials ($P < 0.05$).

and BE-32030 (ref. 37), and the α-methyl-L-Ser antibiotics amicetin and bamicetin[38]. We showed that ObiH catalyzed a retro-aldol reaction on L-Thr, yielding acetaldehyde and a PLP-stabilized glycine enolate that underwent a crossed aldol reaction with PNPAA to yield (2*S*,3*R*)-β-OH-*p*-NO_2-homoPhe, setting the final stereochemistry found in the Obi β-lactone scaffold (**Fig. 2a**; **Supplementary Figs. 6c** and **11**). Double-enzyme reactions with decarboxylase ObiG and aldolase ObiH monitored by LC–MS established that L-Thr is greatly preferred to D-Thr, L-allo-Thr, D-allo-Thr, L-Ser, D-Ser, and Gly as the amino acid substrate (**Supplementary Fig. 10**). The stereochemistry of β-OH-*p*-NO_2-homoPhe matches that of L-Thr, suggesting a preference of this substrate for giving the required enolate stereochemistry for the asymmetric aldol reaction (**Supplementary Fig. 11**). The ObiH PLP cofactor formed a glycine enolate quinonoid intermediate upon exposure to L-Thr, as observed by optical absorption spectroscopy (λ = 495 nm), which was stable throughout the entire protein expression and purification process, including dialysis (**Supplementary Figs. 12** and **13**). Kinetic analysis of the ObiH reaction by ^{1}H-NMR suggested strong product feedback inhibition of ObiH (**Fig. 2d** and **Supplementary Fig. 10**). We hypothesized that downstream utilization of the nonproteinogenic amino acid β-OH-*p*-NO_2-homoPhe by the ATP-consuming NRPS ObiF would drive the ObiH equilibrium toward product.

ObiF is a β-lactone-forming NRPS

The NRPS ObiF is a single-module, 209-kDa protein with C–A–T–TE–A_{Ar} catalytic domains (**Supplementary Figs. 6e**,**f** and **14**), and ObiD is a separate aryl acyl carrier protein (T_{Ar}) (**Supplementary Fig. 6d**). We examined whether recombinant ObiF and ObiD, together, could convert β-OH-*p*-NO_2-homoPhe and 2,3-DHB to Obi (**Fig. 3a**). Prior to running *in vitro* enzyme reactions, we primed recombinant ObiD and ObiF with 4-phosphopantetheine transferase (Sfp) and coenzyme A to install the phosphopantetheine post-translational modification on the T domains. Treatment of β-OH-*p*-NO_2-homoPhe and 2,3-DHB with holo-ObiF and holo-ObiD, together, in the presence of ATP and Mg^{2+} gave clean conversion to the ring-closed Obi β-lactone and the corresponding ring-opened hydrolysis product Obi-COOH, presumably originating from the nonenzymatic hydrolysis of Obi (**Fig. 3b**; **Supplementary Fig. 15**; **Supplementary Table 4**).

Unlike the lipstatin[13], ebelactone[7], salinosporamide[14], and oxazolomycin[15] PKS and NRPS assembly lines, ObiF has a TE domain in the termination module. Primary sequence analysis of the ObiF TE domain revealed that the expected catalytic serine of the conserved GxSxG motif is replaced by a cysteine at residue 1141; this mutation has been found previously in type II TEs but is rarely reported for type I TEs[16,39,40]. We prepared phosphopantetheinylated C1141S and C1141A ObiF variants to test the importance of C1141 in β-lactone formation. The C1141S mutation converted ObiF from a 'β-lactone synthase' to a classic hydrolase that produced only Obi-COOH from the *in vitro* reaction of the holo-ObiF C1141S mutant and holo-ObiD with β-OH-*p*-NO_2-homoPhe and 2,3-DHB (**Fig. 3b**,**c**; **Supplementary Fig. 15**; **Supplementary Table 5**). The C1141A mutation brought the catalytic activity of ObiF to a near halt, with only trace amounts of Obi-COOH detected by LC–MS (**Fig. 3b**,**c**; **Supplementary Fig. 15**; **Supplementary Table 6**). Presumably, the

© 2017 Nature America, Inc., part of Springer Nature. All rights reserved.

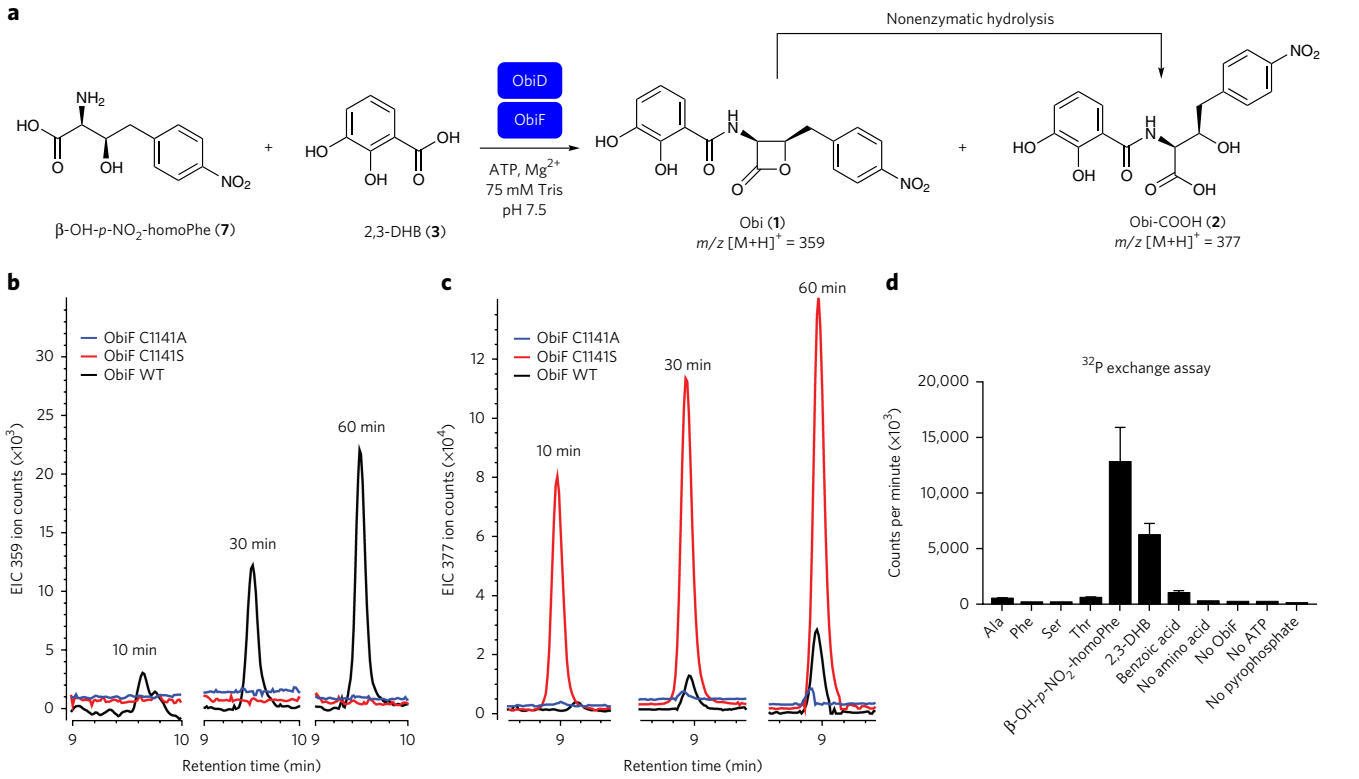

Figure 3 | Enzymatic conversion of β-OH-*p*-NO_2-homoPhe and 2,3-DHB to Obi β-lactone using recombinant NRPS assembly line ObiF and ObiD. (**a**) Scheme depicting the enzymatic conversion of β-OH-*p*-NO_2-homoPhe and 2,3-DHB to Obi (*m/z* = 359 for $[M+H]^+$) and Obi-COOH (*m/z* = 377 for $[M+H]^+$). (**b**) EICs (*m/z* = 359) for reactions of 2,3-DHB, β-OH-*p*-NO_2-homoPhe, and holo-ObiD with holo-ObiF wild type (WT; black), holo-ObiF C1141S mutant (red), and holo-ObiF C1141A mutant (blue). (**c**) EICs (*m/z* = 377) for reactions of 2,3-DHB, β-OH-*p*-NO_2-homoPhe, and holo-ObiD with holo-ObiF WT (black), holo-ObiF C1141S mutant (red), and holo-ObiF C1141A mutant (blue). (**d**) ATP-[^{32}P]PP_i exchange assay to detect carboxylic acid adenylation by ObiF. The graph shows counts per minute (c.p.m.) for each carboxylate substrate. Additional amino acid substrates (Arg, Asn, Asp, Cys, Glu, Gln, Gly, His, Ile, Leu, Lys, Met, Orn, Pro, Trp, Val) are not included in the graph because of the negligible c.p.m. observed for them. Error bars represent s.d. for three independent trials ($P < 0.05$).

penultimate 2,3-DHB-β-OH-*p*-NO_2-homoPhe thioester stalled on the T domain, as acyl transfer to the TE domain of the holo-ObiF C1141A mutant was blocked. The trace Obi-COOH that was detected by LC–MS is predicted to form via slow hydrolysis of the T-domain thioester. Prolonged exposure (24 h) of the holo-ObiF C1141A mutant and holo-ObiD to 2,3-DHB, β-OH-*p*-NO_2-homoPhe, and ATP resulted in steady production of Obi-COOH, supporting the theory that the NRPS module was functional but required slow, nonenzymatic hydrolysis of the 2,3-DHB-β-OH-*p*-NO_2-homoPhe T-domain thioester for turnover. We also expressed, purified, and functionally characterized recombinant ObiF and ObiD homologs from *C. shinanonensis* SAY3 (**Supplementary Fig. 16**; **Supplementary Table 2**). Reaction of holo-ObiF and holo-ObiD from *C. shinanonensis* with β-OH-*p*-NO_2-homoPhe and 2,3-DHB gave enzyme-, time-, and ATP-dependent conversion to Obi and Obi-COOH (**Supplementary Fig. 17**; **Supplementary Table 7**). The ability of recombinant holo-ObiF and holo-ObiD from *C. shinanonensis* to catalyze the *in vitro* conversion of β-OH-*p*-NO_2-homoPhe and 2,3-DHB to Obi with similar efficiency to the *P. fluorescens* enzymes suggests that the NRPS module would be functional when expressed and phosphopantetheinylated in *C. shinanonensis*.

We employed an ATP-[^{32}P]pyrophosphate (PP_i) exchange assay to test for reversible acyl-adenylate intermediate formation and showed that the ObiF A domains are highly selective for the activation of β-OH-*p*-NO_2-homoPhe and 2,3-DHB (**Fig. 3d**). Proteinogenic amino acids, including the β-hydroxy (L-Thr and L-Ser) and aromatic (L-Phe) amino acids, produced signals comparable to those of control reactions lacking an amino acid substrate. Analysis of the ObiF primary sequence with NRPSPredictor2 software predicted that the embedded A domain would adenylate L-Thr and that the terminal A_{Ar} domain would adenylate 2,3-DHB (**Supplementary Table 8**)[41]. The specificity-conferring sequence[42] of the embedded ObiF A domain (D/A/W/G/C/G/L/I) showed similarity to the consensus signature sequences for A domains that activate L-Thr (D/F/W/N/I/G/M/V) and L-Phe (D/A/W/T/I/A/A/V), with some key differences that help account for accommodation of the sterically larger β-OH-*p*-NO_2-homoPhe substrate. In comparison to L-Phe A domains, Thr at position 4 is changed to a Gly, extending the active site pocket to accommodate the chain extended homoPhe. In comparison to L-Thr A domains, Phe at position 2 is changed to Ala, and Asn at position 4 is changed to Gly, which leaves room to accommodate the benzyl group. Both L-Phe and L-Thr A domains have an Ile at position 5, which is changed to Cys in ObiF. The Cys might interact favorably with the electron-deficient nitrophenyl group (**Supplementary Fig. 18**).

β-Lactone formation requires Cys1141

We propose a direct role for the ObiF TE domain in the formation of the Obi β-lactone ring as the final biosynthetic step, releasing the mature cyclized product from the NRPS assembly line. The ObiF 2,3-DHB–β-OH-*p*-NO_2-homoPhe T thioester must be shuttled from the T domain and loaded to the TE domain via energy-neutral transthioesterification, where it resides as the C1141 thioester and undergoes C3-OH-to-C1 cyclization to release Obi β-lactone. The weaker C–S bond of the thioester, compared to the C–O bond of an oxo-ester, is likely required to make strained β-lactone ring

© 2017 Nature America, Inc., part of Springer Nature. All rights reserved.

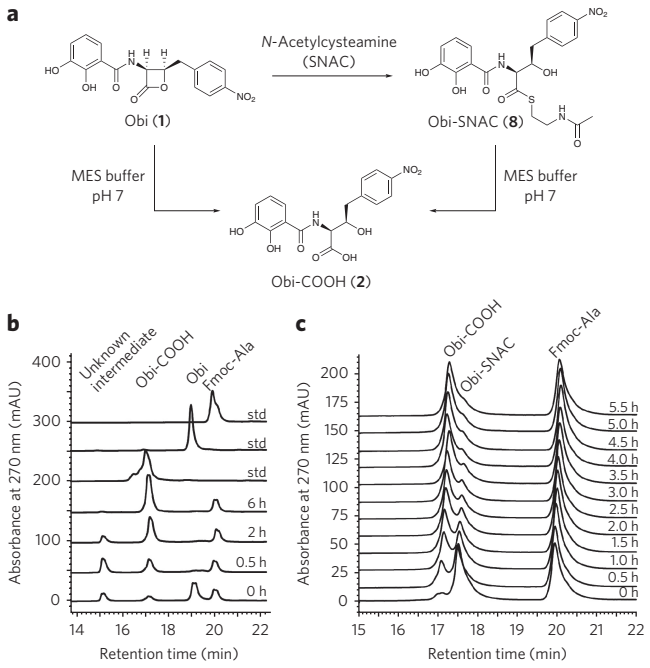

Figure 4 | ObiF catalysis is required for β-lactone ring formation. (**a**) Scheme depicting the synthesis of Obi-*N*-acetylcysteamine (SNAC) and the hydrolysis of Obi and Obi-SNAC to Obi-COOH. Treatment of Obi with neat SNAC results in quantitative conversion to Obi-SNAC. Hydrolysis of Obi (**b**) and Obi-SNAC (**c**) at pH 7 in MES buffer was monitored by HPLC with detection by optical absorbance spectroscopy at 270 nm using an Fmoc-L-Ala internal standard. Peak identities were confirmed using LC–MS and comparison to authentic standards. Std, pure analytical standard. The traces represent single measurements from two independent experiments.

formation thermodynamically favorable[43]. The higher ground state energy of the Cys thioester, compared to that of the Ser oxo-ester, is also predicted to increase the rate of alcohol addition to the carbonyl group, which is likely the rate-determining step. The thermodynamic requirements for β-lactone formation are not met by the oxo-ester intermediate created by the ObiF C1141S mutant, resulting in the accumulation of only the hydrolysis product Obi-COOH (**Fig. 3c**). The ObiF C1141A mutant also failed to generate detectable concentrations of Obi β-lactone, which supports the theory that TE catalysis is required in β-lactone ring formation.

To further probe the role of the TE domain in β-lactone formation, we prepared an *N*-acetylcysteamine (SNAC) thioester (Obi-SNAC, **8**) and compared its rate of hydrolysis with that of Obi β-lactone. Dissolving purified Obi from *P. fluorescens* culture supernatant in neat SNAC thiol resulted in quantitative conversion to Obi-SNAC thioester (**Fig. 4a**; **Supplementary Fig. 19**). We monitored the hydrolysis of Obi (**Fig. 4b**) and Obi-SNAC (**Fig. 4c**) in MES buffer at pH 7 by HPLC with detection by optical absorbance spectroscopy at 270 nm. We observed rapid hydrolysis of Obi in MES buffer at pH 7 with a half-life <30 min and immediate formation of two products (retention times of 15.2 min and 17.2 min) with optical absorbance spectra that are consistent with the presence of an aryl nitro group (**Fig. 4b**). Comparison to an analytical standard of Obi-COOH purified from *P. fluorescens* culture supernatant confirmed the peak at retention time 17.2 min to be Obi-COOH. The peak at retention time 15.2 min is an uncharacterized intermediate that converted directly to Obi-COOH. Previous studies of Obi hydrolysis using ^{1}H-NMR in D_2O/CD_3CN (1:4) showed that an oxazoline intermediate forms and hydrolyzes to give *O*-(2,3-dihydroxybenzoyl)-β-OH-*p*-NO_2-homoPhe[26]. We observed that Obi-SNAC hydrolyzed directly to Obi-COOH in MES buffer at pH 7 with a half-life of 3.2 h (**Fig. 4c**). The rate of Obi-SNAC hydrolysis was comparable to that of the ObiF C1141A mutant (**Fig. 3c**; **Supplementary Fig. 15**), which further supports the role of the ObiF TE domain as a catalyst for β-lactone ring formation.

A model for Obi biosynthesis

Our *in vitro* characterization of ObiD, ObiF, ObiG, ObiH, and ObiL; computational prediction of ObiA, ObiB, ObiC, ObiE, ObiI, ObiJ, and ObiK function; and previously reported isotope labeled precursor studies[27,28] enabled us to propose a complete model for Obi biosynthesis in *P. fluorescens* (**Fig. 5**). Carbon flux to Obi biosynthesis starts from the primary metabolites erythrose-4-phosphate and PEP, which are converted to chorismate by the upregulated DAHP synthase ObiB and the endogenous shikimate pathway. ObiA, ObiC, and ObiE convert chorismate to 2,3-DHB, and ObiI, ObiJ, and ObiK convert it to PAPPA. Aryl amine oxidase ObiL converts PAPPA to PNPPA, and ThDP-dependent decarboxylase ObiG converts PNPPA to PNPAA. Threonine aldolase ObiH establishes equilibrium between PNPAA, L-Thr, acetaldehyde, and β-OH-*p*-NO_2-homoPhe. The ATP-consuming NRPS ObiF activates β-OH-*p*-NO_2-homoPhe as the acyl adenylate with the embedded A domain and covalently loads the amino acid as a phosphopantetheinyl thioester on the embedded T domain. 2,3-DHB is similarly activated as the acyl adenylate by the C-terminal A_{Ar} domain and loaded on the stand-alone T_{Ar} domain ObiD as a phosphopantetheinyl thioester. The C domain is predicted to catalyze amide bond formation between the α-amino group of the ObiF β-OH-*p*-NO_2-homoPhe-T-thioester and the carbonyl of the ObiD 2,3-DHB-T_{Ar}-thioester, releasing free T_{Ar} (ObiD) and forming the 2,3-DHB-β-OH-*p*-NO_2-homoPhe-T-thioester. Transthioesterification to the active site C1141 of the TE domain leads to cyclization of the β-hydroxythioester to the corresponding β-lactone, releasing Obi and turning over the NRPS assembly line for another round of catalysis (**Supplementary Fig. 20**).

DISCUSSION

There are some general features from the ObiF TE domain that might be genetic and biochemical signatures for β-lactone biosynthesis. A GxCxG motif is likely required for β-lactone ring formation. The active site Cys provides a favorable kinetic and thermodynamic scenario for strained-ring formation, proceeding through a more reactive thioester compared to the traditional oxo-ester intermediate. The advantages of activated TE domain thioesters as substrates for NRPS product release might extend to other strained-ring systems including β-lactams. Recently, the biosynthetic gene cluster for the monobactam sulfazecin was reported to encode an NRPS with a terminal type I TE domain that contains an active site Cys residue[44]. GxCxG motifs are rare among type I TE domains[16]. Analysis of the TE protein family (PF00975) revealed that 264 out of 3,863 members (6.8%) contained a GxCxG motif, whereas the remaining 93.2% contained a GxSxG motif. Analysis of the top 20,000 hits from standard protein BLAST search of the full ObiF sequence against nonredundant protein sequences in the NCBI database revealed that 13,944 sequences possessed a GxSxG motif, 1,240 sequences contained a GxCxG motif, and 194 sequences contained a GHCxG motif. Homologous ObiF TE domains from *P. fluorescens*, *C. shinanonensis*, and *B. diffusa* all contain a GHCAG motif and show >50% total sequence homology (**Supplementary Fig. 16**; **Supplementary Table 9**). Comparison to a diverse sampling of PKS and NRPS TE domains, including pyochelin and AB3403 TE domains with GxCxG motifs, showed that the ObiF TE domain is sequence unique (**Supplementary Fig. 21**; **Supplementary Table 10**)[39,40]. Homology modeling predicted overall structural similarities to canonical type I α/β hydrolases, with the conserved Asp residue of the catalytic triad moved from β-strand 6 to β-strand 7 (**Supplementary Fig. 22**)[16]. Future mechanistic and structural studies will help elucidate the catalytic roles of the His–Cys–Asp triad

© 2017 Nature America, Inc., part of Springer Nature. All rights reserved.

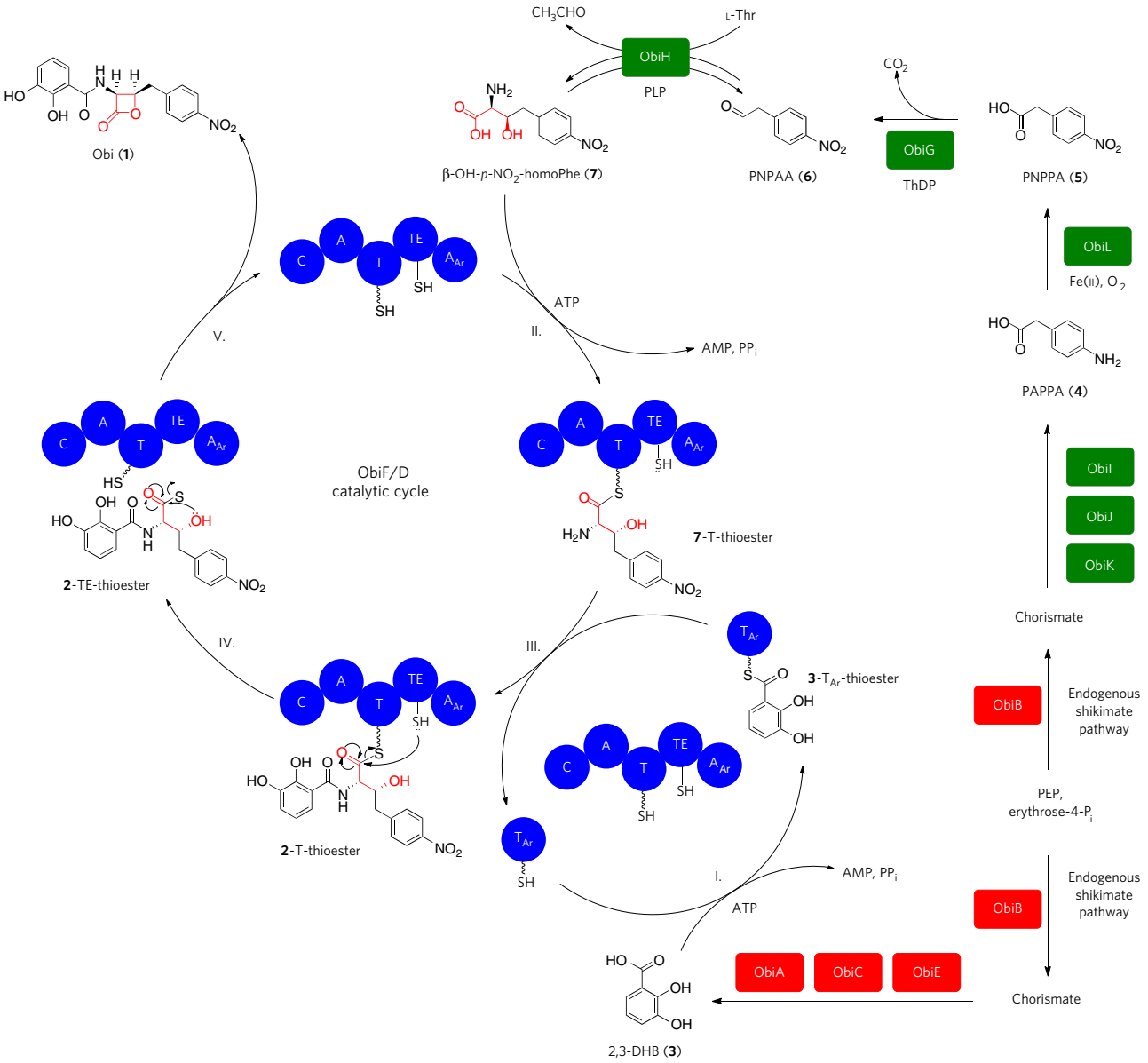

Figure 5 | Model for Obi biosynthesis and the catalytic cycle of NRPS assembly line ObiF. ObiB directs carbon flux from the primary metabolic pool to chorismate via the endogenous shikimate pathway. ObiA, ObiC, and ObiE convert chorismate to 2,3-DHB. ObiI, ObiJ, and ObiK convert chorismate to PAPPA. ObiL converts PAPPA to PNPPA. ObiG converts PNPPA to PNPAA. ObiH establishes equilibrium between L-Thr, PNPAA, acetaldehyde, and β-OH-*p*-NO_2-homoPhe. ObiF and ObiD are the NRPS assembly line components that convert β-OH-*p*-NO_2-homoPhe and 2,3-DHB to Obi at the cost of two ATP molecules. The NRPS catalytic cycle starts (I) with A_{Ar} catalyzed activation and loading of 2,3-DHB to the T_{Ar} domain as the phosphopantetheinyl thioester. Similarly, the ObiF embedded A domain activates and loads β-OH-*p*-NO_2-homoPhe to the ObiF T domain (II). The C domain catalyzes amide bond formation giving the **2**-T-thioester (III). Transthioesterification to active site Cys1141 of the TE domain (IV) leads to cyclization releasing Obi β-lactone (V).

and will clarify whether substrate preorganization plays a role in formation of the strained four-membered β-lactone ring[10,20].

Inclusion of the 2,3-DHB-activating A_{Ar} domain as part of the ObiF NRPS module might be optional. In the *P. fluorescens* and *C. shinanonensis* ObiF NRPSs the A_{Ar} domain is included in the CDS as the C-terminal catalytic domain. In the *B. diffusa* NRPS, the A_{Ar} domain is predicted to be a stand-alone enzyme that activates 2,3-DHB as the acyl adenylate for *in trans* transfer to the T_{Ar} carrier protein in analogy to the enterobactin NRPS machinery (EntF, EntE, and EntB) (**Supplementary Fig. 23**). An MbtH domain is encoded in the ObiF primary sequence between the TE and A_{Ar} domains. The MbtH-like protein YbdZ is encoded in the enterobactin biosynthetic gene cluster and has been shown to enhance the adenylation activity of EntF[45]. The ObiF MbtH-like domain might play a similar role to YbdZ. Recent structural and biophysical studies of NRPS modules with C–A–T–TE domains have provided insight into the motions and dynamics of individual domains during coordinated catalysis by the enzyme assembly lines[40,46]. The TE domain is highly dynamic and is distal from the T domain until invoked for final product release. In the case of ObiF, this would leave A_{Ar} free to catalyze the formation of the 2,3-DHB acyl adenylate and keep the T_{Ar} carrier protein loaded as a 2,3-DHB phosphopantetheinyl thioester. In the case of enterobactin biosynthesis, the A_{Ar} and T_{Ar} domains, EntE and EntB, respectively, are separate from the main NRPS module, EntF, which activates and loads Ser as a T-domain phosphopantetheinyl thioester[45]. The full-length EntF is required for trimerization of Ser,

© 2017 Nature America, Inc., part of Springer Nature. All rights reserved.

amide bond formation with 2,3-DHB, and cyclization to the macrolactone[47]. Thus, only A_{Ar} and T_{Ar} domains have been shown to be active *in trans*, supporting the existence of ObiF NRPS modules with and without the A_{Ar} domain as part of the main NRPS module.

It is conceivable that other catalytic domains with active site Cys residues might catalyze cyclization of β-hydroxythioesters to β-lactones. For example, an uncharacterized ketosynthase (KS) domain resides at the C terminus of the ebelactone PKS termination module[7]. KS domains undergo transthioesterification reactions with T domain thioesters to form intermediate KS-Cys thioesters on a conserved Cys–His–His triad[48]. KS domains typically catalyze thio-Claisen condensations with malonyl T-domain thioesters, but might also be capable of β-lactone ring forming condensations. The termination module of the hybrid PKS–NRPS assembly line for oxazolomycin features a C-terminal C domain of unknown function[15]. Condensation domains typically catalyze amide bond formation between two T domain thioesters, but there are documented cases of C domains catalyzing cyclization during product release such as in cyclosporin A and enniatin biosynthesis[20]. The oxazolomycin terminal C domain might catalyze the intramolecular condensation of a T domain thioester to the spirocyclic β-lactone. The salinosporamide biosynthetic gene cluster encodes for several uncharacterized enzymes, including a standalone KS domain, SalC, that might participate in bicyclic β-lactone formation[4,14]. We predict that more β-lactone-forming "logic gates" will be discovered as part of NRPS–PKS modular assembly lines and possibly as autonomous catalysts[10,16,49].

Obi represents a novel structural class of β-lactone antibiotics from nature's chemical inventory. The Obi biosynthetic machinery characterized in this study offers a versatile platform for the chemoenzymatic synthesis of β-lactones from β-hydroxy-α-amino acid precursors. Here, the new amino acid β-OH-*p*-NO_2-homoPhe was produced by a threonine aldolase, possibly representing a general strategy for producing β-hydroxy-α-amino acid precursors to peptide β-lactones. Fe(II)/α-KG-dependent oxygenases and non-heme di-iron oxygenases are also known to produce β-hydroxy-α-amino acids via direct C–H bond activation chemistry on free amino acids[50,51]. Hydroxylation of amino acid side chains can also take place while loaded as thioesters on NRPS T domains, making A domain substrate prediction insufficient for the potential incorporation of β-hydroxy-α-amino acids into NRP scaffolds[52]. Our work shows that β-hydroxy-α-amino acids can be directly incorporated into peptide scaffolds on an NRPS assembly line, leading to peptides capped at the C terminus with a β-lactone warhead. Our genetic and biochemical characterization of the Obi biosynthetic pathway in *P. fluorescens* will guide future genome mining efforts and expands the known chemistry of NRPS and PKS product release mechanisms to include strained 4-membered ring formation[10,20,24]. Our chemoenzymatic approach to C-terminal β-lactone peptides has the potential for applications in precursor-directed feeding studies and NRPS engineering to produce targeted peptide β-lactone inhibitors of proteases for the treatment of diseases associated with microbial and viral infections[5,6,25], cancer[4], and obesity[3].

Received 1 June 2016; accepted 7 March 2017;
published online 15 May 2017

METHODS

Methods, including statements of data availability and any associated accession codes and references, are available in the online version of the paper.

References

1. Lowe, C. & Vederas, J.C. Naturally occuring β-lactones: occurence, synthesis and properties. A review. *Org. Prep. Proced. Int.* **27**, 305–346 (1995).
2. Bachovchin, D.A. *et al.* Superfamily-wide portrait of serine hydrolase inhibition achieved by library-versus-library screening. *Proc. Natl. Acad. Sci. USA* **107**, 20941–20946 (2010).
3. Pemble, C.W. IV, Johnson, L.C., Kridel, S.J. & Lowther, W.T. Crystal structure of the thioesterase domain of human fatty acid synthase inhibited by Orlistat. *Nat. Struct. Mol. Biol.* **14**, 704–709 (2007).
4. Gulder, T.A. & Moore, B.S. Salinosporamide natural products: Potent 20S proteasome inhibitors as promising cancer chemotherapeutics. *Angew. Chem. Int. Edn Engl.* **49**, 9346–9367 (2010).
5. De Pascale, G., Nazi, I., Harrison, P.H. & Wright, G.D. β-Lactone natural products and derivatives inactivate homoserine transacetylase, a target for antimicrobial agents. *J. Antibiot. (Tokyo)* **64**, 483–487 (2011).
6. Lall, M.S., Ramtohul, Y.K., James, M.N.G. & Vederas, J.C. Serine and threonine β-lactones: a new class of hepatitis A virus 3C cysteine proteinase inhibitors. *J. Org. Chem.* **67**, 1536–1547 (2002).
7. Wyatt, M.A. *et al.* Biosynthesis of ebelactone A: isotopic tracer, advanced precursor and genetic studies reveal a thioesterase-independent cyclization to give a polyketide β-lactone. *J. Antibiot. (Tokyo)* **66**, 421–430 (2013).
8. Hamed, R.B. *et al.* The enzymes of β-lactam biosynthesis. *Nat. Prod. Rep.* **30**, 21–107 (2013).
9. Roach, P.L. *et al.* Structure of isopenicillin N synthase complexed with substrate and the mechanism of penicillin formation. *Nature* **387**, 827–830 (1997).
10. Bachmann, B.O., Li, R. & Townsend, C.A. β-Lactam synthetase: a new biosynthetic enzyme. *Proc. Natl. Acad. Sci. USA* **95**, 9082–9086 (1998).
11. Gaudelli, N.M., Long, D.H. & Townsend, C.A. β-Lactam formation by a non-ribosomal peptide synthetase during antibiotic biosynthesis. *Nature* **520**, 383–387 (2015).
12. Christenson, J.K. *et al.* β-Lactone synthetase found in the olefin biosynthesis pathway. *Biochemistry* **56**, 348–351 (2017).
13. Bai, T. *et al.* Operon for biosynthesis of lipstatin, the β-lactone inhibitor of human pancreatic lipase. *Appl. Environ. Microbiol.* **80**, 7473–7483 (2014).
14. Eustáquio, A.S. *et al.* Biosynthesis of the salinosporamide A polyketide synthase substrate chloroethylmalonyl-coenzyme A from *S*-adenosyl-L-methionine. *Proc. Natl. Acad. Sci. USA* **106**, 12295–12300 (2009).
15. Zhao, C. *et al.* Oxazolomycin biosynthesis in *Streptomyces albus* JA3453 featuring an "acyltransferase-less" type I polyketide synthase that incorporates two distinct extender units. *J. Biol. Chem.* **285**, 20097–20108 (2010).
16. Horsman, M.E., Hari, T.P. & Boddy, C.N. Polyketide synthase and nonribosomal peptide synthetase thioesterase selectivity: logic gate or a victim of fate? *Nat. Prod. Rep.* **33**, 183–202 (2016).
17. Jiang, Y., Morley, K.L., Schrag, J.D. & Kazlauskas, R.J. Different active-site loop orientation in serine hydrolases versus acyltransferases. *ChemBioChem* **12**, 768–776 (2011).
18. Gaudelli, N.M. & Townsend, C.A. Epimerization and substrate gating by a TE domain in β-lactam antibiotic biosynthesis. *Nat. Chem. Biol.* **10**, 251–258 (2014).
19. Jensen, K. *et al.* Polyketide proofreading by an acyltransferase-like enzyme. *Chem. Biol.* **19**, 329–339 (2012).
20. Kopp, F. & Marahiel, M.A. Macrocyclization strategies in polyketide and nonribosomal peptide biosynthesis. *Nat. Prod. Rep.* **24**, 735–749 (2007).
21. Dick, L.R. *et al.* Mechanistic studies on the inactivation of the proteasome by lactacystin: a central role for clasto-lactacystin β-lactone. *J. Biol. Chem.* **271**, 7273–7276 (1996).
22. Wells, J.S., Trejo, W.H., Principe, P.A. & Sykes, R.B. Obafluorin, a novel β-lactone produced by *Pseudomonas fluorescens*. Taxonomy, fermentation and biological properties. *J. Antibiot. (Tokyo)* **37**, 802–803 (1984).
23. Tymiak, A.A., Culver, C.A., Malley, M.F. & Gougoutas, J.Z. Structure of obafluorin: an antibacterial β-lactone from *Pseudomonas fluorescens*. *J. Org. Chem.* **50**, 5491–5495 (1985).
24. Dejong, C.A. *et al.* Polyketide and nonribosomal peptide retro-biosynthesis and global gene cluster matching. *Nat. Chem. Biol.* **12**, 1007–1014 (2016).
25. Hamed, R.B. *et al.* Crotonase catalysis enables flexible production of functionalized prolines and carbapenams. *J. Am. Chem. Soc.* **134**, 471–479 (2012).
26. Pu, Y., Lowe, C., Sailer, M. & Vederas, J.C. Synthesis, stability, and antimicrobial activity of (+)-obafluorin and related β-lactone antibiotics. *J. Org. Chem.* **59**, 3642–3655 (1994).
27. Herbert, R.B. & Knaggs, A.R. Biosynthesis of the antibiotic obafluorin from D-[U-^{13}C]glucose and *p*-aminophenylalanine in *Pseudomonas fluorescens*. *J. Chem. Soc. Perkin Trans. I* **1992**, 103–107 (1992).
28. Herbert, R.B. & Knaggs, A.R. Biosynthesis of the antibiotic obafluorin from p-aminophenylalanine and glycine (glyoxylate). *J. Chem. Soc. Perkin Trans. I* **1992**, 109–113 (1992).
29. Bentley, R. The shikimate pathway—a metabolic tree with many branches. *Crit. Rev. Biochem. Mol. Biol.* **25**, 307–384 (1990).
30. Walsh, C.T., Liu, J., Rusnak, F. & Sakaitani, M. Molecular studies on enzymes in chorismate metabolism and the enterobactin biosynthetic pathway. *Chem. Rev.* **90**, 1105–1129 (1990).
31. Fernández-Martínez, L.T. *et al.* New insights into chloramphenicol biosynthesis in *Streptomyces venezuelae* ATCC 10712. *Antimicrob. Agents Chemother.* **58**, 7441–7450 (2014).

© 2017 Nature America, Inc., part of Springer Nature. All rights reserved.

32. Blanc, V. *et al.* Identification and analysis of genes from *Streptomyces pristinaespiralis* encoding enzymes involved in the biosynthesis of the 4-dimethylamino-L-phenylalanine precursor of pristinamycin I. *Mol. Microbiol.* **23**, 191–202 (1997).
33. Choi, Y.S., Zhang, H., Brunzelle, J.S., Nair, S.K. & Zhao, H. In vitro reconstitution and crystal structure of *p*-aminobenzoate N-oxygenase (AurF) involved in aureothin biosynthesis. *Proc. Natl. Acad. Sci. USA* **105**, 6858–6863 (2008).
34. Makris, T.M. *et al.* An unusual peroxo intermediate of the arylamine oxygenase of the chloramphenicol biosynthetic pathway. *J. Am. Chem. Soc.* **137**, 1608–1617 (2015).
35. Contestabile, R. *et al.* L-Threonine aldolase, serine hydroxymethyltransferase and fungal alanine racemase. A subgroup of strictly related enzymes specialized for different functions. *Eur. J. Biochem.* **268**, 6508–6525 (2001).
36. Barnard-Britson, S. *et al.* Amalgamation of nucleosides and amino acids in antibiotic biosynthesis: discovery of an L-threonine:uridine-5′-aldehyde transaldolase. *J. Am. Chem. Soc.* **134**, 18514–18517 (2012).
37. Muliandi, A. *et al.* Biosynthesis of the 4-methyloxazoline-containing nonribosomal peptides, JBIR-34 and -35, in *Streptomyces* sp. Sp080513GE-23. *Chem. Biol.* **21**, 923–934 (2014).
38. Zhang, G. *et al.* Characterization of the amicetin biosynthesis gene cluster from *Streptomyces vinaceusdrappus* NRRL 2363 implicates two alternative strategies for amide bond formation. *Appl. Environ. Microbiol.* **78**, 2393–2401 (2012).
39. Reimmann, C., Serino, L., Beyeler, M. & Haas, D. Dihydroaeruginoic acid synthetase and pyochelin synthetase, products of the pchEF genes, are induced by extracellular pyochelin in *Pseudomonas aeruginosa*. *Microbiology* **144**, 3135–3148 (1998).
40. Drake, E.J. *et al.* Structures of two distinct conformations of holo-non-ribosomal peptide synthetases. *Nature* **529**, 235–238 (2016).
41. Röttig, M. *et al.* NRPSpredictor2—a web server for predicting NRPS adenylation domain specificity. *Nucleic Acids Res.* **39**, W362–W367 (2011).
42. Challis, G.L., Ravel, J. & Townsend, C.A. Predictive, structure-based model of amino acid recognition by nonribosomal peptide synthetase adenylation domains. *Chem. Biol.* **7**, 211–224 (2000).
43. McGrath, N.A. & Raines, R.T. Chemoselectivity in chemical biology: acyl transfer reactions with sulfur and selenium. *Acc. Chem. Res.* **44**, 752–761 (2011).
44. Li, R., Oliver, R.A. & Townsend, C.A. Identification and characterization of the sulfazecin monobactam biosynthetic gene cluster. *Cell Chem. Biol.* **24**, 24–34 (2017).
45. Miller, B.R., Drake, E.J., Shi, C., Aldrich, C.C. & Gulick, A.M. Structures of a nonribosomal peptide synthetase module bound to MbtH-like proteins support a highly dynamic domain architecture. *J. Biol. Chem.* **291**, 22559–22571 (2016).
46. Reimer, J.M., Aloise, M.N., Harrison, P.M. & Schmeing, T.M. Synthetic cycle of the initiation module of a formylating nonribosomal peptide synthetase. *Nature* **529**, 239–242 (2016).
47. Ehmann, D.E., Shaw-Reid, C.A., Losey, H.C. & Walsh, C.T. The EntF and EntE adenylation domains of *Escherichia coli* enterobactin synthetase: sequestration and selectivity in acyl-AMP transfers to thiolation domain cosubstrates. *Proc. Natl. Acad. Sci. USA* **97**, 2509–2514 (2000).
48. Smith, S. & Tsai, S.C. The type I fatty acid and polyketide synthases: a tale of two megasynthases. *Nat. Prod. Rep.* **24**, 1041–1072 (2007).
49. Kohli, R.M., Takagi, J. & Walsh, C.T. The thioesterase domain from a nonribosomal peptide synthetase as a cyclization catalyst for integrin binding peptides. *Proc. Natl. Acad. Sci. USA* **99**, 1247–1252 (2002).
50. Makris, T.M., Chakrabarti, M., Münck, E. & Lipscomb, J.D. A family of di-iron monooxygenases catalyzing amino acid β-hydroxylation in antibiotic biosynthesis. *Proc. Natl. Acad. Sci. USA* **107**, 15 391–15396 (2010).
51. Jiang, W. *et al.* EcdGHK are three tailoring iron oxygenases for amino acid building blocks of the echinocandin scaffold. *J. Am. Chem. Soc.* **135**, 4457–4466 (2013).
52. Haslinger, K. *et al.* The structure of a transient complex of a nonribosomal peptide synthetase and a cytochrome P450 monooxygenase. *Angew. Chem. Int. Edn Engl.* **53**, 8518–8522 (2014).

Acknowledgments

This work was supported with start-up funds provided by Washington University in St. Louis and the Research Corporation for Science Advancement through a Cottrell Scholar award to T.A.W. We thank C.T. Walsh (Stanford ChEM-H) for productive scientific discussions. We thank Cofactor Genomics (St. Louis, MO) for bioinformatics consultation and genome sequence analysis. We thank S. Alvarez and B. Evans at the Proteomics & Mass Spectrometry Facility at the Donald Danforth Plant Science Center (St. Louis, MO) for the acquisition of high-resolution MS spectra (NSF Grant No. DBI-0922879). We thank J.-S. Taylor (WUSTL Department of Chemistry) for assistance with the [^{32}P]PP$_i$ exchange assay. We thank J. Kao (WUSTL Department of Chemistry) for assistance with NMR experiments.

Author Contributions

T.A.W., J.E.S., and M.R.R. wrote the paper and prepared the supplementary information. T.A.W. oversaw all of the experiments. J.E.S. and M.R.R. cloned and purified ObiG, ObiH, and ObiL. J.E.S. functionally characterized ObiG, ObiH, and ObiL. M.R.R. cloned, purified, and functionally characterized ObiD and ObiF. J.E.S. and M.R.R. purified and characterized all compounds. T.A.W. and N.K.P. isolated *Pseudomonas fluorescens* gDNA, analyzed sequencing data, and annotated the Obi biosynthetic gene cluster. N.K.P. performed protein homology modeling and helped with preparation of the supplementary information.

Competing financial interests

The authors declare no competing financial interests.

Additional information

Any supplementary information, chemical compound information and source data are available in the online version of the paper. Reprints and permissions information is available online at http://www.nature.com/reprints/index.html. Publisher's note: Springer Nature remains neutral with regard to jurisdictional claims in published maps and institutional affiliations. Correspondence and requests for materials should be addressed to T.A.W.

© 2017 Nature America, Inc., part of Springer Nature. All rights reserved.

© 2017 Nature America, Inc., part of Springer Nature. All rights reserved.

ONLINE METHODS

Strains, materials, and instrumentation. *P. fluorescens* ATCC 39502 was purchased from ATCC, and glycerol stocks were made from cells grown in Bennett's media and stored at −80 °C. DNA primers were purchased from Integrated DNA Technologies. Herculase II DNA polymerase kit was purchased from Agilent. T4 DNA ligase and NheI were purchased from New England BioLabs. T4 Polynucleotide Kinase and FastDigest (FD) restriction enzymes NdeI, HindII, and DpnI were purchased from Thermo Scientific. TOP10 *Escherichia coli* cells were purchased from Invitrogen and BL21-Gold(DE3) *E. coli* cells were purchased from Agilent. PCR was performed on a Bio-Rad MyCycler thermal cycler. Nickel-nitrilotriacetic acid (Ni-NTA) agarose was purchased from Invitrogen. Any kD SDS–PAGE gels were purchased from Bio-Rad. Plasmid DNA sequencing was performed by Genewiz. Buffers, salts, and chemical reagents were purchased from Sigma-Aldrich, unless otherwise stated. Fully deuterated MES buffer and D_2O were purchased from Cambridge Isotope Laboratories. PAPPA was purchased from Tractus Chemistry. PNPPA was purchased from Frinton Laboratories, Inc. PPA and phenazine methosulfate were purchased from Acros Organics. ^{32}P- radiolabeled sodium pyrophosphate was purchased from PerkinElmer. Samples for HPLC and LC–MS were prepared in 0.45 µm PTFE MiniUniPrep vials from Agilent. All pH measurements were recorded using an Orion Star A111 pH meter and a PerpHecT ROSS micro combination pH electrode from Thermo Scientific. Analytical HPLC was performed using Beckman Coulter SYSTEM GOLD 126 solvent module, 508 autosampler, and 168 detector with a Phenomenex Luna 5 µm C18(2) 100A column, 250 × 4.6 mm with guard column. All preparatory HPLC was performed using a Beckman Coulter SYSTEM GOLD 127P solvent module and 168 detector with a Phenomenex Luna 10u C18(2) 100A column, 250 × 21.20 mm, 10 µm with guard column. Analytical and prep HPLC were performed with mobile phases of 0.1% TFA in (A) water and (B) acetonitrile, and data were processed using 32 Karat software, version 7.0. Low-resolution LC–MS was performed on an Agilent 6130 single quadrupole LC–MS with G1313 autosampler, G1315 diode array detector, and 1200 series solvent module. A Phenomenex Gemini C18 column, 50 × 2 mm, 5 µm with guard column was used for LC–MS separations. LC–MS mobile phases were 0.1% formic acid in (A) water and (B) acetonitrile, and data were processed using G2710 ChemStation software. NMR was performed on Varian Unity Plus-300 MHz, Varian Unity Inova-500 MHz, and Varian Unity-600 MHz (with cold probe) instruments. Optical absorption spectroscopy was performed on a Cary 50 fit with an autosampler and water Peltier thermostat system using 1 cm quartz cuvettes. High-resolution MS spectra were collected using an LTW-Velos Pro Orbitrap at the Donald Danforth Plant Science Center, St. Louis, MO.

Sequencing of *P. fluorescens* ATCC 39502 Genomic DNA. The *P. fluorescens* ATCC 39502 gDNA was isolated using a Qiagen DNeasy Blood & Tissue kit following the provided instructions. The gDNA was sequenced by Ambry Genetics (Aliso Viejo, CA) using Illumnia MiSeq. Contigs containing ORFs were assembled, annotated, and deposited in GenBank (Accession #s KX134682–KX134695) with assistance from Cofactor Genomics (St. Louis, MO).

Cloning, expression, and purification of ObiG, ObiH, ObiL, ObiD, ObiF, ObiF C1141S, ObiF C1141A, CS-ObiD and CS-ObiF. Gene sequences were amplified from either *P. fluorescens* ATCC 39502 gDNA or *C. shinanonensis* DSM 23277 (CS) gDNA (isolated using Qiagen DNeasy Blood & tissue kit following provided instructions) using forward and reverse primers designed for each gene (**Supplementary Tables 11–13**) and a Herculase II Fusion DNA Polymerase kit. The resulting PCR fragments were purified by gel electrophoresis. PCR products and pET28a vector were separately digested with either FD-NdeI and FD-HindIII or NheI and FD-HindIII. Cut DNA was purified using a QIAquick Gel Extraction Kit. Ligation reactions were carried out overnight at 16 °C using T4 DNA Ligase. Ligation mixtures were purified and transformed into electrocompetent *E. coli* TOP10 cells. Clones were selected for on LB agar containing 50 µg/ml kanamycin. Sequencing of selected colonies revealed clones containing the desired constructs. Plasmids were purified and used to transform electrocompetent *E. coli* BL21 (DE3) cells.

For protein expression, a 5 ml culture of *E. coli* BL21 harboring the appropriate plasmid was grown overnight in LB containing 50 µg/ml kanamycin with agitation at 37 °C. A 200 µl aliquot of this culture was used to inoculate 500 ml of terrific broth (12 g/L tryptone, 24 g/L yeast extract, 5 g/L glycerol, 17 mM KH_2PO_4, and 72 mM K_2HPO_4) containing 50 µg/ml kanamycin. The culture was grown at 37 °C with agitation until OD_{600} reached approximately 0.4. The culture was cooled in an ice bath for 20 min, then 500 µl of a sterile 0.5 M IPTG solution was added. Culture was then incubated with agitation for 18 h (at 15 °C for ObiG/ObiF/CS-ObiF, and at 20 °C for ObiD/CS-ObiD/ObiH/ObiL). From this point on, all protein purification steps were performed at 4 °C. Cells were harvested by centrifugation at 5,000 r.p.m. for 20 min. Supernatant was discarded, and cell pellets were each suspended in 40 ml cold lysis buffer (50 mM K_2HPO_4 pH 8.0, 500 mM NaCl, 5 mM β-mercaptoethanol, 20 mM imidazole, and 10% glycerol). Cell suspensions were transferred to 50 ml Falcon tubes and flash frozen in liquid nitrogen. Frozen cells were thawed and gently rocked for 30 min before being mechanically lysed using an Avestin EmulsiFlex-C5 cell disruptor. Cell lysate was centrifuged at 45,000 r.p.m. for 35 min and supernatant was incubated with pre-washed Ni-NTA resin for 30 min. Resin was washed twice with 40 ml lysis buffer and then eluted five times with 10 ml elution buffer (50 mM K_2HPO_4 pH 8.0, 500 mM NaCl, 5 mM β-mercaptoethanol, 300 mM imidazole, and 10% glycerol). Fractions containing the majority of protein, as judged by SDS–PAGE with Coomassie blue visualization (**Supplementary Fig. 5**), were combined in 10,000 MWCO SnakeSkin dialysis tubing from Thermo Scientific and soaked overnight in 1.8 L phosphate buffer (50 mM K_2HPO_4 pH 8.0, 150 mM NaCl, 1 mM DTT). Dialyzed protein solution was concentrated using an appropriately sized spin filter (EMD Millipore Amicon Ultra 15 ml Centrifugal Filters). Concentrated protein solutions were flash frozen in liquid nitrogen and stored at −80 °C.

Mutagenesis of WT-ObiF to ObiF C1141S and ObiF C1141A. Mutagenesis primers (**Supplementary Tables 11** and **12**) were phosphorylated using T4 Polynucleotide Kinase according to product instructions. Primers were taken directly from the phosphorylation mixture for use in PCR amplification. PCR was carried out using a Herculase II Fusion DNA Polymerase kit. After amplification, 1 µl FastDigest DpnI was added to PCR reaction mixture to digest template plasmid with wild-type gene. The reaction was incubated at 37 °C for 60 min, and plasmids were then purified using gel electrophoresis. Purified plasmids were ligated overnight at 16 °C using T4 DNA ligase, then transformed into electrocompetent *E. coli* TOP10 cells. Plasmids were sequenced to confirm the desired mutations.

ObiG Purpald reactions. A pre-incubation solution was made with 10 µM ThDP, 10 µM $MgCl_2$, 25 mM MES buffer pH 7.5, and 10 µM ObiG from a freshly thawed frozen stock. The enzyme pre-incubation solution incubated at room temperature for 5 min. In a separate 1.5 ml Eppendorf tube, the pyruvic acid substrate (PAPPA, PNPPA, PHPPA, or PPA) was diluted to 1 mM in 25 mM MES pH 7.5 buffer. The substrate mix was transferred in one aliquot into the pre-incubation solution. The final concentrations of reagents were 10 µM ObiG, 5 µM ThDP, 5 µM $MgCl_2$, 1 mM pyruvic acid substrate, and 25 mM MES buffer pH 7.5. Aliquots of the enzyme solution were added to an equal volume of a 20 mg/ml solution of Purpald in 1 M aqueous NaOH at various time points. The resulting solution was mixed and then left open to air to develop the purple color (**Supplementary Fig. 9**). All reactions and time points were single trials.

Detection of ObiH quinonoid by optical absorption spectroscopy. In a 1.5 ml Eppendorf tube, a master mix of 50 µM ObiH from a freshly thawed frozen stock, 50 µM PLP, and 25 mM MES buffer was prepared and analyzed by optical absorption spectroscopy scanning from 200 to 600 nm. Three solutions at a final volume of 500 µl were analyzed as single trials: (1) L-Thr was added to the master mix a 1 mM final concentration; (2) PAA was added to the master mix at 1 mM final concentration; (3) L-Thr and PAA were added to the master mix at 1 mM final concentration each. Samples were then analyzed by optical absorption spectroscopy scanning from 200–600 nm in order to observe the quinonoid peak, which absorbs at ~495 nm (**Supplementary Fig. 12**).

Combined ObiG and ObiH double enzyme reactions. Three solutions were prepared using individual Eppendorf tubes. First, an ObiG solution containing

© 2017 Nature America, Inc., part of Springer Nature. All rights reserved.

10 μM ThDP, 10 μM $MgCl_2$, and 10 μM ObiG was adjusted to 333 μl final volume using 25 mM MES buffer pH 7.5 and allowed to pre-incubate for 5 min. Second, a pyruvic acid solution, 1 mM final concentration, was adjusted to 333 μl with 25 mM MES buffer pH 7.5. Third, an ObiH solution containing 10 μM PLP, 1 mM amino acid (L-Thr, D-Thr, L-Ser, D-Ser, Gly, L-alloThr, or D-alloThr), and 10 μM ObiH was adjusted to 333 μl final volume. After the pre-incubation time was complete, the three solutions were combined in a single Eppendorf tube and allowed to rest for 3 h at room temperature before quenching with MeCN to crash the enzyme. The mixtures were centrifuged and the supernatants were analyzed by LC–MS using a gradient of 0% B held for 5 min then 0% B to 95% B over 10 min using single ion monitoring for the expected ions in positive ion mode (retention times and observed product ions: β-OH-homoPhe, 1.7 min, $[M+H]^+$ = 196; β-OH-*p*-OH-homoPhe, 0.8 min, $[M+H]^+$ = 212; β-OH-*p*-NO_2-homoPhe, 2.9 min, $[M+H]^+$ = 241; β-OH-*p*-NH_2-homoPhe, not observed; **Fig. 2c** and **Supplementary Fig. 10**). Product masses were confirmed by high-resolution LC–MS analysis. For NMR analysis the same samples were prepared using fully deuterated MES buffer. After equilibration for 3 h, the reactions were quenched with TFA to a pH ~2. The samples were then flash frozen in liquid nitrogen, lyophilized to dryness, resuspended in 750 μl of D_2O, and centrifuged to pellet any insoluble particulate. The soluble supernatants were then transferred to NMR tubes and analyzed (**Fig. 2d**; **Supplementary Fig. 10**). All reactions were performed in triplicate.

Purification of β-OH-*p*-NO_2-homoPhe from the ObiG/ObiH reaction. The ObiG/ObiH double-enzyme reaction described above was scaled up with respect to the substrates to produce enough material for NMR analysis. The concentrations of reaction components were 10 μM ObiG, 10 μM ThDP, 10 μM $MgCl_2$, 10 μM ObiH, 10 μM PLP, 5 mM L-Thr, 5 mM PNPPA, and 25 mM pH 7.5 MES buffer, with a final reaction volume of 1 ml. After 3 h the reaction was quenched with TFA to a pH ~2, centrifuged at 13,000 r.p.m. for 2 min, flash frozen in liquid nitrogen, and lyophilized to dryness. The resulting solid was dissolved in 1:10 MeCN:H_2O, filtered, and purified by preparatory HPLC using a solvent gradient of 0% B held for 5 min then 0% B to 100% B over 10 min (β-OH-*p*-NO_2-homoPhe retention time = 14.3 min). The desired TFA salt of β-OH-*p*-NO_2-homoPhe product was isolated as a white powder. ^{1}H NMR (500 MHz, D_2O) δ (p.p.m) = 8.24 (d, *J* = 8.4 Hz, 2 H), 7.55 (d, *J* = 9.0 Hz, 2 H), 4.49 – 4.43 (ddd, *J* = 3.6, 4.8, 10.2 Hz, 1 H), 3.98 (d, *J* = 4.8 Hz, 1 H), 3.20 (dd, *J* = 3.6, 14.4 Hz, 1 H), 2.99 (dd, *J* = 10.2, 13.8 Hz, 1 H); ^{13}C NMR (126 MHz, D_2O) δ (p.p.m.) = 160.6, 136.0, 134.9, 119.7, 113.2, 59.1, 47.5, 28.9; HRMS (ESI) calculated for $C_{10}H_{11}N_2O_5$: 241.0819 [$(M+H)^+$], found peak when extracting ions for 241.0795–241.0843. See **Supplementary Note** for tabulated NMR data and copies of spectra.

Combined ObiG, ObiH, and ObiL triple enzyme reaction. A solution of 100 μM ObiL from a freshly thawed frozen stock, 3 mM phenazine methosulfate (PMS), 1 mM PAPPA, 100 μM iron(II) sulfate, and 25 mM NADH was prepared in 25 mM MES buffer at pH 5.5 at a final volume of 500 μl (refs. 33,53). NADH was added last to initiate the reaction and the mixture was incubated at room temperature for 1 h. Upon addition of NADH, the color of the reaction changed from light yellow to sky blue (**Supplementary Fig. 7**). In a separate Eppendorf tube, a 500 μl solution was prepared containing 10 μM ObiG, 10 μM ThDP, 10 μM $MgCl_2$, 10 μM ObiH, 10 μM PLP, 1 mM L-Thr, and 25 mM MES buffer at pH 7. The pH of the ObiL solution changed from 5.5 to 7.0 over the course of the reaction. The control assay reached an end pH of 6.0 and was adjusted to a pH of 7 using 1 M NaOH before addition of the ObiG/ObiH solution. The ObiG/ObiH solution was added directly to the ObiL solution, allowed to react for 2 h at room temperature, and quenched with MeCN to crash the enzymes. The mixtures were centrifuged and the supernatants were analyzed by LC–MS using a gradient of 0% B held for 5 min then 0% B to 95% B over 10 min. Ion counts for expected products were extracted from total ion chromatograms in positive ion mode (**Fig. 2b**; retention times and observed product ions: β-OH-*p*-NO_2-homoPhe, 1.7 min, $[M+H]^+$ = 241). The β-OH-*p*-NO_2-homoPhe ion was confirmed by HRMS. Reaction was performed as two independent trials.

Combined ObiF and ObiD double enzyme reaction. Phosphopantetheinylation of apo-ObiD and apo-ObiF (wild type, C1141S and C1141A mutants, and *C. shinanonensis* homologs) was carried out in separate 500 μl solutions containing 180 μM CoASH, 5 mM DTT, 10 mM $MgCl_2$, 400 nM Sfp, 25 μM apo enzyme, and 75 mM Tris–HCl at pH 7.5 (ref. 54). Reactions were left at room temperature for 2 h, and then used directly as the source of holo-ObiD and holo-ObiF. Reactions were performed in duplicate at 500 μl total volume. Full reactions contained 5 mM ATP, 5 mM DTT, 1 mM 2,3-DHB, 1 mM β-OH-*p*-NO_2-homoPhe, 1 μM holo-ObiF (ObiF, CS-ObiF, ObiF-C1141A, or ObiF-C1141S), 1 μM holo-ObiD, and 75 mM Tris–HCl at pH 7.5. For reactions with CS-ObiF, the holo-ObiD homolog from *C. shinanonensis* (CS-ObiD) was used as the aryl acyl adenylating enzyme. Control reactions were also prepared by replacing various components with an equivalent volume of 75 mM Tris–HCl buffer. Three control experiments were performed for the ObiF, ObiF-C1141S, ObiF-C1141A, CS-ObiF reactions: (–) ObiD; (–) 2,3-DHB/(–) β-OH-*p*-NO_2-homoPhe; and (–) ATP. Two additional controls were prepared as either (–) ObiF or (–) ObiF/(–) ObiD (**Supplementary Tables 4–7**). Reactions were performed at room temperature. At 10, 30, and 60 min time points, a 50 μl aliquot from each reaction was quenched with 50 μl acidic MeCN (acidified with HCl) to give a final pH of approximately 3.5. Mixtures were centrifuged for 2 min at 13,000 r.p.m. to remove precipitated enzyme, and the supernatants were analyzed by LC–MS using a gradient of 5% solvent B to 95% solvent B over 20 min. Ion counts for Obi and Obi-COOH were extracted from total ion chromatograms in positive ion mode (retention times and observed ions: Obi, 9.5 min, $[M+H]^+$ = 359; Obi-COOH, 9.0 min, $[M+H]^+$ = 377) (**Fig. 3b**,**c**). Reaction mixtures were also analyzed by HPLC using a gradient of 5% B to 95% B over 20 min, 95% B to 100% B over 3 min, and 100% B to 5% B over 2 min at a flow rate of 1 ml/min with optical absorbance detection at 270 nm (**Supplementary Fig. 15**). Product ions and retention times were confirmed using purified standards of Obi and Obi-COOH isolated from *P. fluorescens* ATCC 39502 fermentations (**Supplementary Fig. 19**).

[^{32}P]PPi exchange assay. Reaction mixtures (650 μl) contained 2 μM ObiF, 5 mM acid substrate, 1 mM ATP, 1 mM $MgCl_2$, 40 mM KCl, 1 mM DTT, 5 mM Na[^{32}P]PP_i (3.3×10^5 c.p.m./ml), and 50 mM Tris–HCl (pH 8)[55]. Mixtures were incubated at room temperature for 30 min, then three 200 μl aliquots were removed and each were quenched with 500 μl of a charcoal suspension (100 mM $NaPP_i$, 350 mM $HClO_4$, and 16 g/L powdered charcoal). The mixtures were shaken, then centrifuged at 13,000 r.p.m. for 3 min. Charcoal pellets were washed with 750 μl of wash solution (100 mM $NaPP_i$, 350 mM $HClO_4$) and centrifuged again for 3 min. Washing step was repeated once more, followed by suspension of charcoal pellets in 1.5 ml EcoLite(+) scintillation fluid from MP Biomedicals. Charcoal-bound radioactivity was measured on a Beckman Coulter LS 6500 scintillation counter. Graph of results indicates measured c.p.m. (**Fig. 3d**). All proteinogenic amino acids were L-stereoisomers.

Isolation of Obi and Obi-COOH. Obi and the hydrolysis product Obi-COOH were isolated from *Pseudomonas fluorescens* ATCC 39502 fermentations as previously described[22,23]. Bennet's Agar slants (1 g/L yeast extract, 1 g/L beef extract, 2 g/L NZ amine, 10 g/L glucose, 15 g/L agar) were inoculated with streaks of *P. fluorescens* ATCC 39502 from a frozen glycerol stock. The slants were incubated at 25 °C for 48 h. 5 ml of sterile saline was added to the top of the slant and shaken gently. Inoculated saline (1 mL) was transferred to 100 ml of sterile media (5 g/L yeast extract, 5 g/L glucose, 0.1 g/L $MgSO_4{\cdot}7H_2O$, 0.1 g/L $FeSO_4{\cdot}7H_2O$, 200 ml soil filtrate extract from campus of Washington University in St. Louis, 800 ml tap water, autoclaved). This starter culture was incubated with shaking at 225 r.p.m. at 25 °C for 24 h. 5 ml of starter culture was transferred to each 3 L baffled flask containing 500 ml of the same media, and the cultures were incubated with shaking at 225 r.p.m. at 25 °C for 17 h. The cultures were pooled and centrifuged at 5,000 r.p.m. at 4 °C for 25 min to pellet cells. The supernatant was pooled and acidified to pH 3 with 1M aqueous HCl. The pooled supernatant was saturated with EtOAc then extracted with three 100 ml volumes of EtOAc. Extractions were pooled and dried using rotary evaporation to yield a gray-brown solid. The solid was dissolved in 10 ml acetonitrile, filtered, and concentrated by rotary evaporation under reduced pressure to yield 221 mg of clear, brown oil. The oil was dissolved in 10 ml of acetonitrile, filtered, and purified with Prep HPLC with a gradient of 5% solvent B to 95% solvent B over 20 min. The two largest peaks were isolated

doi:10.1038/nchembio.2374

which upon NMR analysis proved to be Obi (retention time = 23.0 min) and Obi-COOH (retention time = 20.5 min), both isolated as brown oils. Obi: ^{1}H NMR (500 MHz, methanol-d_4) δ (p.p.m.) = 8.12 (d, *J* = 9.0 Hz, 2 H), 7.49 (d, *J* = 8.4 Hz, 2 H), 7.28 (d, *J* = 9.6 Hz, 1 H), 6.99 (d, *J* = 6.6 Hz, 1 H), 6.78 (t, *J* = 1.0 Hz, 1 H), 5.83 (d, *J* = 6.0 Hz, 1 H), 5.08 (td, *J* = 5.7, 9.0 Hz, 1 H), 3.40 (dd, *J* = 9.0, 15.0 Hz, 1 H), 3.21 (dd, *J* = 5.1, 14.7 Hz, 1 H); ^{13}C NMR (126 MHz, methanol-d_4) δ (p.p.m.) = 171.8, 170.2, 150.5, 148.7, 147.8, 145.8, 131.6, 130.5, 129.9, 128.1, 124.9, 120.8, 120.4, 119.5, 116.4, 79.2, 60.5, 36.8; HRMS (ESI) calculated for $C_{17}H_{15}N_2O_7$: 359.0874 [(M+H)$^+$], found peak when extracting ions for 359.0858–359.0930. See **Supplementary Note** for tabulated NMR data and copies of spectra. Obi-COOH: ^{1}H NMR (500 MHz, methanol-d_4) δ (p.p.m.) = 8.15 (d, *J* = 8.4 Hz, 2 H), 7.50 (d, *J* = 8.4 Hz, 2 H), 7.37 (d, *J* = 9.6 Hz, 1 H), 6.98 (d, *J* = 9.0 Hz, 1 H), 6.78 (t, *J* = 8.1 Hz, 1 H), 4.75 (d, *J* = 2.4 Hz, 1 H), 4.54 (ddd, *J* = 2.1, 5.6, 8.0 Hz, 1 H), 3.03 (t, *J* = 1.0 Hz, 1 H), 2.96 (t, *J* = 1.0 Hz, 1 H); ^{13}C NMR (126 MHz, methanol-d_4) δ (p.p.m.) = 173.8, 170.7, 149.3, 148.3, 147.8, 147.4, 131.8, 124.7, 124.6, 124.5, 120.2, 120.1, 120.0, 117.8, 73.3, 63.4, 57.7, 41.8; HRMS (ESI) calculated for $C_{17}H_{15}N_2O_8$: 375.0834 [(M+H)$^+$], found peak when extracting ions for 375.0796–375.0872. See **Supplementary Note** for tabulated NMR data and copies of spectra. See **Supplementary Figure 19** for LC–MS analysis of *P. fluorescens* culture supernatant, purified Obi, and purified Obi-COOH.

Synthesis of Obi-SNAC. 1 mg purified Obi β-lactone was dissolved in 5 mg SNAC. The solution was left at room temperature overnight, and then diluted with 0.5 ml MeCN and purified by reverse phase preparatory HPLC (gradient of 5% B to 95% B over 20 min at flow rate of 10 ml/min). Product-containing fraction (retention time 21.2 min) was concentrated by rotary evaporation, dissolved in 0.5 ml DMSO, and transferred to a 1.5 ml Eppendorf tube. Solution was lyophilized overnight and dissolved in methanol-d_4 for NMR analysis. Obi-SNAC forms a 2:1 mixture of rotamers in methanol-d_4. The NMR data for the major rotamer is given below. ^{1}H NMR (600 MHz, methanol-d_4) δ (p.p.m.) = 9.08 (d, *J* = 8.7 Hz, 1 H), 8.13 (d, *J* = 8.7 Hz, 1 H), 7.48 (d, *J* = 7.9 Hz, 1 H), 7.41 (d, *J* = 7.9 Hz, 1 H), 6.99 (d, *J* = 7.9 Hz, 1 H), 6.80 (t, *J* = 7.9 Hz, 1 H), 4.75 (d, *J* = 8.7 Hz, 1 H), 4.59 (t, *J* = 6.7 Hz, 1 H), 3.05 – 2.94 (m, 4 H), 1.89 (s, 3 H); ^{13}C NMR (151 MHz, methanol-d_4) δ (p.p.m.) = 201.7, 170.3, 148.6, 148.2, 147.3, 147.2, 131.7, 124.4, 120.8, 120.2, 119.9, 72.7, 64.2, 41.6, 39.8, 29.4, 22.5; LC-MS (ESI) calculated for $C_{21}H_{24}N_3O_8S$: 478.1 [(M+H)$^+$], found: 478.1 (retention time 9.1 min). See **Supplementary Note** for tabulated NMR data and copies of spectra. See **Supplementary Figure 19** for LC–MS analysis of purified Obi-SNAC.

Hydrolysis of Obi and Obi-SNAC to Obi-COOH. Solutions of purified Obi (1 mM) and Obi-SNAC (1 mM) were prepared in MES buffer at pH ~7. Aliquots (100 µl) were taken at various time points analyzed by HPLC (gradient of 5% B to 95% B over 20 min, 95% B to 100% B over 3 min, and 100% B to 5% B over 2 min at a flow rate of 1 ml/min) with detection by optical absorbance spectroscopy at 270 nm (**Fig. 4b**,**c**). HPLC peak identities were confirmed by LC–MS and retention times were normalized using an Fmoc-Ala internal standard. Experiments were performed in duplicate.

Data availability. *P. fluorescens* ATCC 39502 sequencing data for the Obi biosynthetic gene cluster is deposited in GenBank (Accession numbers KX134682, KX134683, KX134684, KX134685, KX134686, KX134687, KX134688, KX134689, KX134690, KX134691, KX134692, KX134693, KX134694, KX134695). All other data supporting the findings of this study are contained in the published article (and its supplementary information files) or are available from the corresponding author upon request.

53. Chanco, E., Choi, Y.S., Sun, N., Vu, M. & Zhao, H. Characterization of the N-oxygenase AurF from *Streptomyces thioletus*. *Bioorg. Med. Chem.* **22**, 5569–5577 (2014).
54. Quadri, L.E. *et al.* Characterization of Sfp, a *Bacillus subtilis* phosphopantetheinyl transferase for peptidyl carrier protein domains in peptide synthetases. *Biochemistry* **37**, 1585–1595 (1998).
55. Hollenhorst, M.A., Clardy, J. & Walsh, C.T. The ATP-dependent amide ligases DdaG and DdaF assemble the fumaramoyl-dipeptide scaffold of the dapdiamide antibiotics. *Biochemistry* **48**, 10467–10472 (2009).

© 2017 Nature America, Inc., part of Springer Nature. All rights reserved.